Experimental observation of delay-induced radio frequency chaos in a transmission line oscillator

Jonathan N. Blakely and Ned J. Corron

Citation: Chaos: An Interdisciplinary Journal of Nonlinear Science **14**, 1035 (2004); doi: 10.1063/1.1804092
View online: http://dx.doi.org/10.1063/1.1804092
View Table of Contents: http://scitation.aip.org/content/aip/journal/chaos/14/4?ver=pdfcov
Published by the AIP Publishing

Experimental observation of delay-induced radio frequency chaos in a transmission line oscillator

Jonathan N. Blakely and Ned J. Corron
US Army Research, Development, and Engineering Command, AMSRD-AMR-WS-ST, Redstone Arsenal, Alabama 35898

(Received 2 June 2004; accepted 18 August 2004; published online 29 October 2004)

We report an experimental study of fast chaotic dynamics in a delay dynamical system. The system is an electronic device consisting of a length of coaxial cable terminated on one end with a diode and on the other with a negative resistor. When the negative resistance is large, the system evolves to a steady state. As the negative resistance is decreased, a Hopf bifurcation occurs. By varying the length of the transmission line we observe Hopf frequencies from 7–53 MHz. With the transmission line length fixed, we observe a period doubling route to chaos as the negative resistance is further reduced providing the first experimental confirmation of an existing theoretical model for nonlinear dynamics in transmission line oscillators [Corti *et al.*, IEEE Trans. Circ. Syst., I: Fundam. Theory Appl. **41**, 730 (1994)]. However, other experimental results indicate limitations to this model including an inability to predict the Hopf frequency or to produce realistic continuous wave forms. We extend the model to include finite bandwidth effects present in a real negative resistor. The resulting model is a neutral delay differential equation that provides better agreement with experimental results. © *2004 American Institute of Physics*. [DOI: 10.1063/1.1804092]

Complex oscillations are often displayed by systems subject to delayed feedback. Delay-induced dynamics are particularly important in technologies where high-speed operation is necessary. For example, the design of interconnects in modern high-speed computers must take into account transmission line effects including propagation delay to prevent undesirable self-oscillations. Also, many interesting practical applications of chaos, such as communications, require oscillators implemented for radio frequency or microwave operation where circuit design typically involves coping with propagation delays. In this paper, we examine the dynamics of an extremely simple system that displays fast delay-induced chaotic dynamics. The system consists of a standard coaxial cable terminated at one end with a *pn* junction diode and at the other end with a negative resistor. We compare our experimental observations to previous theoretical predictions and find qualitative agreement. However, we show that an extension to the existing theory which adds the effects of a finite bandwidth to the negative resistor more accurately reproduces our experimental results.

INTRODUCTION

Chaos arises in many physical systems due to the effect of delayed feedback. Examples include semiconductor lasers,[1] microwave devices,[2] and electronic circuits.[3] Delayed dynamical systems evolve in an infinite dimensional phase space that on the one hand allows for a wide variety of interesting nonlinear behavior, but on the other hand makes theoretical analysis challenging. For this reason, the understanding of chaotic delay dynamical systems lags that of ordinary dynamical systems.[4] Efforts in recent years to close this gap are driven, in part, by promising applications of high speed chaos such as communication,[2,5–7] noise generation,[3] dynamic memory,[8–10] and random signal radar/ladar.[11,12] In these applications, where ever faster oscillations are sought, delay dynamics arise inevitably as the time it takes for signals to propagate through components becomes comparable to the time scale of fluctuations.[13] Thus a need exists for methods of generating,[14] characterizing,[15] and manipulating[16] fast chaos in delay systems.

In this paper, we experimentally investigate a fast delay dynamical system: a nonlinear transmission line oscillator. By the term *transmission line oscillator* we mean a transmission line terminated with a small number of lumped parameter components including a nonlinear device (as opposed to more complicated systems that contain one or more transmission lines[17,18]). Various nonlinear terminating elements have been studied including a tunnel diode,[19] simple *pn* junction diode,[20–22] and Chua's diode.[23,24] Networks of such oscillators are of technological interest as models of interconnections between modern high-speed integrated circuits.[25,26] Chaos in transmission line oscillators has been predicted theoretically and simulated numerically.[20–24]

The primary result we report here is the first experimental observation of chaos in a transmission line oscillator. The oscillator we examine consists of a transmission line terminated with a diode on one end and a negative resistor on the other. Our observations confirm the presence of chaos as well as the predicted period doubling route to chaos.[20,21] However, we find that important aspects of the observed dynamics cannot be accounted for by the existing theoretical model because it neglects the finite bandwidth of the negative resistor. Therefore, we introduce a new model that includes this important effect and find better agreement with the dynamics of the experimental system.

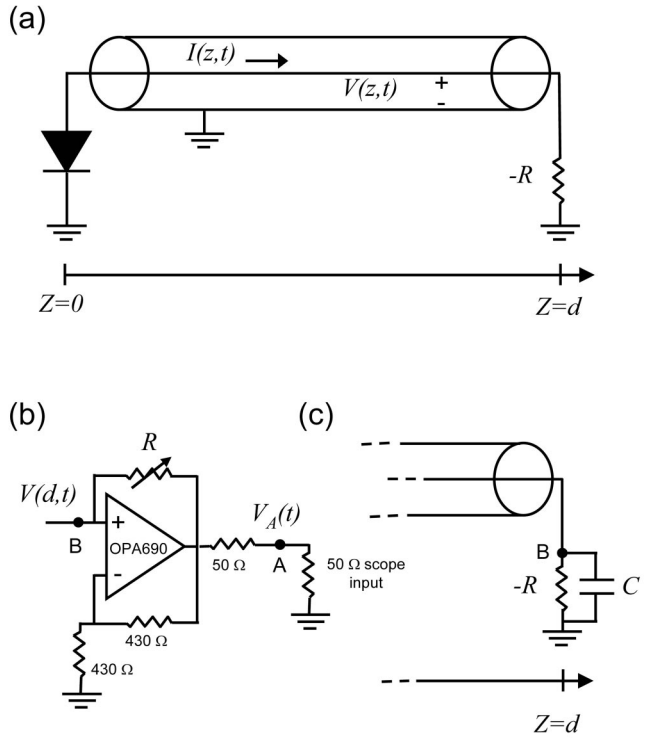

FIG. 1. (a) Schematic of a transmission line nonlinear oscillator. A coaxial cable is terminated on one end with a diode and on the other end with a negative resistor. (b) Circuit diagram of a negative resistor. The nominal value of the negative resistance is determined by the variable resistor R. The voltage at node A is connected to the 50 ohm input of a fast digital oscilloscope. In numerical simulations, the voltage at node B is modeled. (c) The finite bandwidth of the negative resistor is modeled by an ideal capacitor C in parallel with an ideal negative resistor $-R$.

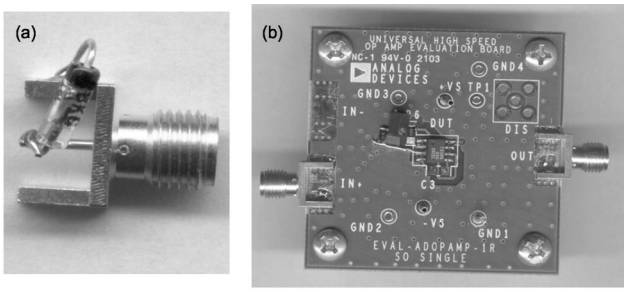

FIG. 2. Photographs showing circuit layout and construction techniques for the terminating devices in the transmission line oscillator. (a) The diode is soldered directly to an SMA connector. (b) The negative resistor circuit is constructed on a commercial evaluation board. A wire (visible to the left of the op amp) was used to connect the feedback from the op amp output to the noninverting input. Otherwise all connections are made through the traces printed on the board.

EXPERIMENTAL OBSERVATIONS

Figure 1(a) shows a schematic of the transmission line oscillator studied here. One end of the line is terminated by a *pn*-junction diode that provides the sole nonlinearity in the system. The other end is terminated by an active circuit known as a "negative resistor."[27] Ideally, this device obeys Ohm's law with resistance $-R$ where the negative sign indicates a current flowing in the opposite direction to that of a normal resistor. Loosely speaking, chaos arises in the system when voltage waves are "stretched" upon reflection from the negative resistor and then "folded" by the nonlinearity of the diode. The time delay is necessary since the terminations alone do not contain enough degrees of freedom to produce chaos. The propagation of waves in both directions in the transmission line gives this system a distinct topology from other delay line oscillators found in the literature, in which waves only propagate in one direction.[1,28,29] This difference has a practical consequence. In one-way systems, unintended reflections off nonlinear components may produce unwanted waves traveling in the wrong direction. This problem is avoided in the present system because reflections are inherently part of the dynamics.

In our experimental system, the transmission line is a length of RG-58/U coaxial cable (Belden 9310) with characteristic impedance $R_c=50$ ohms and a wave speed $v_0=1.97\times10^8$ m/s. The diode (1N34A, Radio Shack cat. no. 276-1123), chosen for its relatively low junction capacitance (typically 0.8 pF according to specifications) and low turn-on voltage (typically $\sim$0.3 volts), is soldered directly to an SMA connector as shown in Fig. 2(a). To obtain dynamics at technologically relevant frequencies, the negative resistor is implemented with high-frequency surface mount components including a high-speed voltage-feedback op amp (OPA690, nominal large-signal bandwidth of 200 MHz) on a universal amplifier evaluation printed circuit board (Analog Devices EVAL-ADOPAMP-1R). A circuit diagram of the negative resistor is shown in Fig. 1(b) and a photograph of the experimental implementation is shown in Fig. 2(b). The negative resistor is a noninverting amplifier with an additional feedback loop. Therefore we choose values of the 430 ohm resistors according to the recommendations in the OPA690 data sheet for a noninverting amplifier with a gain of 2. A variable resistor (BC Components SM4W101) is used to tune R, the magnitude of the negative resistance. The evaluation board does not provide a path for the additional feedback loop so we used a short ($\sim$1 cm) wire [visible in Fig. 2(b)] to connect the resistance R to the op amp noninverting input and output.

We use a fast digital oscilloscope (Tektronix TDS680B) with 50 ohm input impedance to record $V_A(t)$, the voltage following the 50 ohm resistor at the output of the operational amplifier [node A in Fig. 1(b)]. The 50 ohm resistor serves to isolate the amplifier from the capacitive load of the oscilloscope input. Assuming ideal amplifier operation, the voltage $V_A(t)$ is equal to $V(d,t)$.

To characterize the performance of the negative resistor, we observe the reflection of incident waves. According to standard transmission line theory,[22] the reflection coefficient ρ for waves incident on an ideal negative resistor (whose impedance is $-R$) is

$$\rho=\frac{-R-R_c}{-R+R_c}. \tag{1}$$

Figure 3 shows the measured reflection coefficient (squares) as a function of frequency at (a) $R=77$ ohms and (b) $R=101$ ohms, as well as the ideal theoretical value (dotted line). [See the inset to Fig. 3(b) and the caption for details on

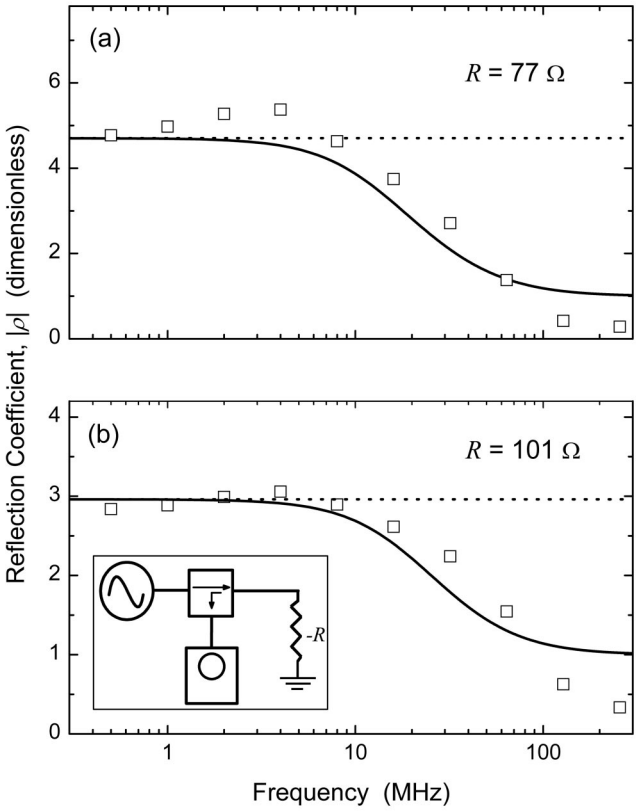

FIG. 3. Frequency dependence of the reflection coefficient of the negative resistor with resistance (a) −77 Ω and (b) −103 Ω. The squares are experimental data points measured using the setup shown in the inset. A function generator provides the incident wave while a directional coupler (Mini-Circuits ZDC-10-1) routes the reflected wave to an oscilloscope. The dotted line shows the response of an ideal negative resistor with infinite bandwidth. The solid line shows the response of the band-limited negative resistor model.

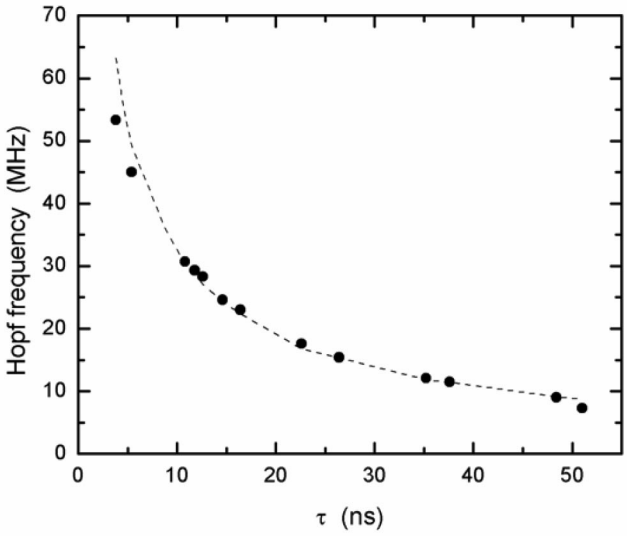

FIG. 4. Dependence of Hopf frequency on time delay τ as observed in the experiment (circles) and in simulation (dashed line).

the experimental setup for this measurement.] At frequencies below a few tens of megahertz, the experimental data agrees well with the ideal model. The measured reflection falls 3 dB below that of the ideal model at around 20 MHz in Fig. 3(a) and 30 MHz in Fig. 3(b).

We observe the dynamics of the experimental system as we vary R, the magnitude of the negative resistance. As R approaches R_c from above, reflected waves are amplified with increasing gain. With a large value of R, the system resides in a steady state. As R decreases towards R_c, a supercritical Hopf bifurcation gives rise to a periodic oscillation. In Fig. 4, we show the dependence of the frequency at the Hopf bifurcation on the time delay, which we observe by changing the length of the coaxial cable. The various lengths of cable used to produce this data range from 37 cm, producing a 53 MHz oscillation, to 5 m, producing a 7 MHz oscillation. We note that by using a faster op amp and a shorter transmission line the results obtained here should scale directly to technologically relevant VHF and UHF frequencies.[29]

Beyond the Hopf bifurcation, we observe a period doubling route to chaos. Figure 5 shows several representative time series of the voltage across the negative resistor at different points along the route to chaos with the fixed delay time of $\tau = 14.6$ ns (or cable length of 1.44 m). Period-one [Fig. 5(a), $R = 86.3$ ohms], period-two [Fig. 5(b), $R = 84.8$ ohms], and period-four [Fig. 5(c), $R = 82.9$ ohms] orbits are resolvable before the onset of chaos [Fig. 5(d), $R = 80.5$ ohms]. It is apparent from the chaotic time series shown in Fig. 5(d) that a strong frequency component near the frequency appearing at the Hopf bifurcation persists even into the chaotic regime. Although it is beyond the scope of the current report, we note that we have also observed more complex, high dimensional chaos when the delay time is longer, consistent with behavior seen in other delay systems.[30,31]

THEORETICAL ANALYSIS

Our observation of a period-doubling route to chaos confirms earlier theoretical predictions and numerical simulations of the dynamics of the transmission line oscillator.[20,21] We now describe briefly the model giving rise to these predictions and its limitations. We then introduce a new model that more successfully reproduces our observations.

Following Corti *et al.*,[20,21] we assume the coaxial cable is a lossless transmission line with characteristic impedance R_c and wave speed v_0. The voltage $V(z,t)$ and current $I(z,t)$ at each point along the line are then governed by the "Telegrapher's equations,"[22]

$$R_c \frac{\partial I(z,t)}{\partial t} = -v_0 \frac{\partial V(z,t)}{\partial z}, \tag{2}$$

$$\frac{\partial V(z,t)}{\partial t} = -v_0 R_c \frac{\partial I(z,t)}{\partial z}, \tag{3}$$

the general solution of which is

$$V(z,t) = \psi^R\left(t - \frac{z}{v_0}\right) + \psi^L\left(t + \frac{z}{v_0}\right), \tag{4}$$

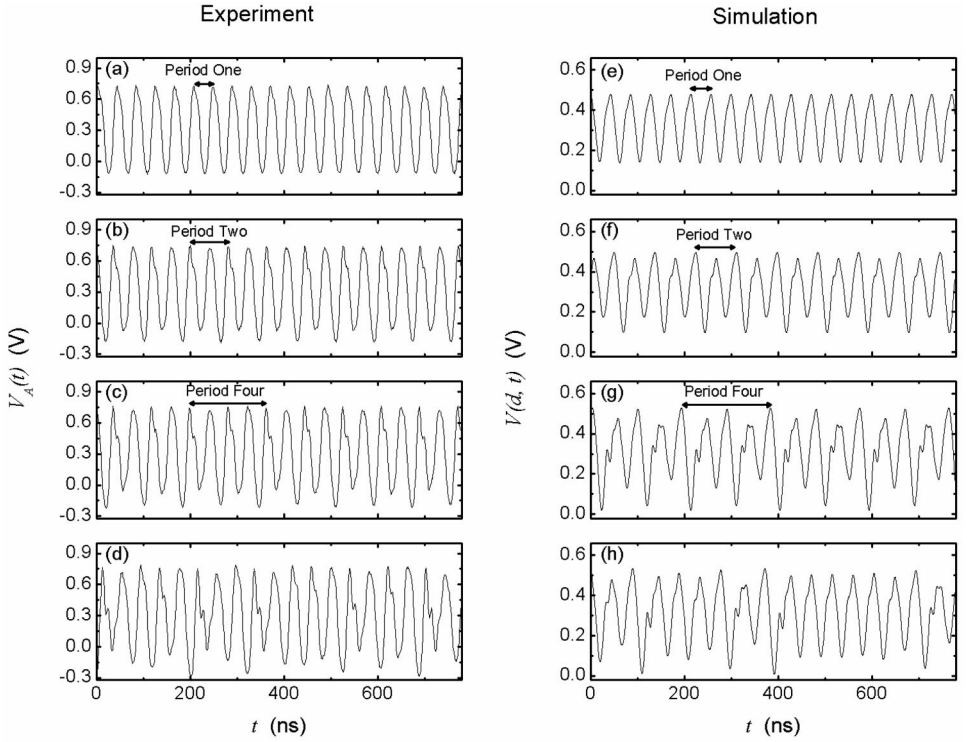

FIG. 5. Observed period doubling route to chaos in the experiment (left) and the simulation (right) with a time delay of 14.6 ns. Periods 1, 2, and 4 are resolvable in the experiment at negative resistance values of (a) $R=86.3$ ohms, (b) $R=84.8$ ohms, (c) $R=82.9$ ohms. In (d), a typical chaotic wave form is shown where $R=80.5$ ohms. Comparable time series produced by simulation when the negative resistance is (e) $R=82$ ohms, (f) $R=80$ ohms, (g) $R=75.6$ ohms, (h) $R=75$ ohms.

$$I(z,t)=\frac{1}{R_c}\left\{\psi^R\left(t-\frac{z}{v_0}\right)-\psi^L\left(t+\frac{z}{v_0}\right)\right\}, \tag{5}$$

where ψ^R is a voltage wave traveling to the right and ψ^L is a voltage wave traveling to the left. The spatial coordinate z is defined as shown in Fig. 1(a).

The equations governing the current and voltage at the terminations constitute boundary conditions for the Telegrapher's equations. At $z=0$, we assume an exponential diode model which yields the boundary condition

$$-I(0,t)=I_s(e^{V(0,t)/V_0}-1), \tag{6}$$

where I_s and V_0 are constants defining the saturation current and turn-on voltage, respectively. Inserting solutions (4) and (5) into (6) gives an implicit relation between ψ^R and ψ^L

$$-\frac{1}{R_c}\{\psi^R(t)-\psi^L(t)\}=I_s(e^{(\psi^R(t)+\psi^L(t))/V_0}-1), \tag{7}$$

which, in the parameter range of interest, has a unique nonzero solution,

$$\psi^R(t)=g[\psi^L(t)]. \tag{8}$$

The unimodal function g is the "folding" nonlinearity in the system (see Ref. 21 for a typical plot of g). At $z=d$, an ideal negative resistor is described by Ohm's law

$$V(d,t)=-RI(d,t). \tag{9}$$

Inserting solutions (4) and (5) into (9) and combining the result with (8) gives the difference equation

$$\psi^L(t)=\left(\frac{R+R_c}{R-R_c}\right)g[\psi^L(t-\tau)], \tag{10}$$

where $\tau=2d/v_0$. The solution to Eq. (10), via Eqs. (4), (5), and (8), then gives a complete solution to the Telegrapher's equations [Eqs. (2) and (3)] with boundary conditions given by Eqs. (7) and (9).

Since the value of $\psi^L(t_1)$ (the wave amplitude at some time t_1) depends only on $\psi^L(t_1-\tau)$ and is completely independent of a value $\psi^L(t_0)$ no matter how close t_0 is to t_1, the model allows for instantaneous finite jumps in the value of $\psi^L(t)$. This instantaneous response, or equivalently infinite bandwidth, is not physically realistic. Nonetheless, useful information about the physical system can be obtained from the difference equation model. First, we find Eq. (10) can accurately reproduce the observed steady state behavior of the system preceding the Hopf bifurcation. Over the range of experimentally accessible values of negative resistance, the experimental and theoretical fixed point values agree to within 1% when $I_s=8$ μA and $V_0=55$ mV. Second, we find the model predicts the correct type of route to chaos. Figure 6 shows a bifurcation diagram for the model where the initial function at each value of negative resistance is a constant, $\psi^L(t)=0.03$, $t\in[-\tau,0]$. In agreement with previous reports, the model predicts a period doubling route to chaos.[20,21]

However, Eq. (10) fails to reproduce many aspects of the experimentally observed dynamics. It cannot produce realistic continuous chaotic wave forms of the type shown in Fig. 5. It produces a route to chaos that occurs over a range of negative resistances from -120 to -95 ohms, somewhat larger values than observed experimentally (-90 to -80 ohms). Finally, at the Hopf bifurcation it predicts oscillations with a period that is a multiple of τ, inconsistent with the data in Fig. 4. We find that these aspects of the dynamics can be more accurately reproduced by incorporating a finite bandwidth into Eq. (10).

The nonphysical bandwidth of the map model can be attributed to Eqs. (6) and (9) describing the diode and negative resistor, respectively. An instantaneous response is as-

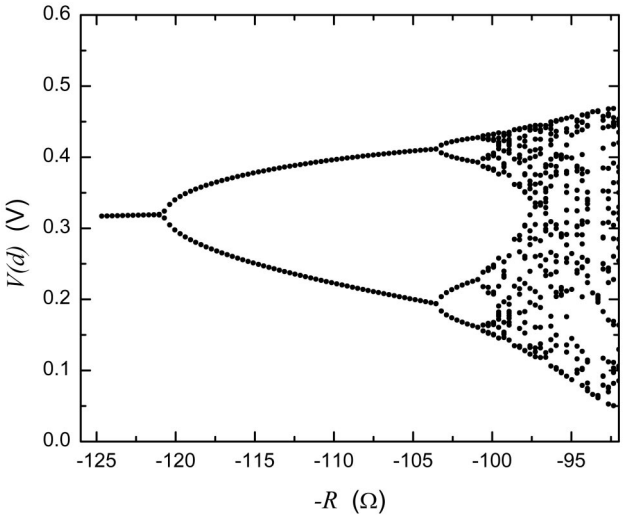

FIG. 6. Bifurcation diagram showing period doubling route to chaos predicted by the map model [Eq. (10)] of the transmission line oscillator.

sumed for both of these components. In reality, neither of these devices respond instantaneously. The bandwidth of the op amp is necessarily limited by an internal capacitance. The printed circuit board on which the negative resistor is implemented and the connector to which the diode is mounted give rise to parasitic reactance further limiting the response of the system. In principle, each nonideal reactance could be modeled separately, however the resulting model would likely be quite complicated. Therefore, we incorporate a finite bandwidth by adding a single, lumped capacitance C in parallel with the ideal negative resistance $-R$ as shown in Fig. 1(c). Any change in the voltage across the negative resistor can only occur at a rate consistent with the finite charging time of the capacitor. Then, at $z=d$, the more realistic boundary condition is

$$C\frac{dV(d,t)}{dt} = I(d,t) + \frac{V(d,t)}{R}. \tag{11}$$

Imposing this new boundary condition along with (6), the dynamics are now described by

$$C\dot{\psi}^L(t) = -\left(\frac{1}{R_c} - \frac{1}{R}\right)\psi^L(t) + \left(\frac{1}{R_c} + \frac{1}{R}\right)g[\psi^L(t-\tau)] - Cg'[\psi^L(t-\tau)]\dot{\psi}^L(t-\tau), \tag{12}$$

where

$$g'[\psi] = \frac{dg}{d\psi}. \tag{13}$$

Equation (12) is a type of functional differential equation known as a neutral differential equation because it includes a time derivative of ψ^L evaluated at the delayed time $t-\tau$.[32] Chaos in such systems has not received much attention in the literature.[33] Note that in the limit where $C\to 0$ this equation reduces to Eq. (10).

We numerically integrate Eq. (12) to compare the new model to the experimental results reported above. The functions g and g' are approximated by polynomials fit to the numerical solutions of Eq. (7). The method of integration is a third order Adams–Bashforth–Moulton predictor–corrector.[34] In order to evaluate the derivative $\dot{\psi}^L(t)$ during each integration step, we need the value of $\psi^L(t-\tau)$ and $\dot{\psi}^L(t-\tau)$. We use a fixed integration step size chosen such that an integer number of steps equals τ. We can then store the values of $\psi^L(t)$ and $\dot{\psi}^L(t)$ in memory for use in future integration steps.

For all parameter values examined, the route to chaos begins, as in the experiment, with a steady state. The steady state of the new model [Eq. (12)] is identical to the steady state of the map model [Eq. (10)]. Therefore, we retain the parameters of the diode model extracted from measurements of the steady state (i.e., $I_s=8$ μA and $V_0=55$ mV). Also as in the experiment, a Hopf bifurcation occurs as the negative resistance is increased. We find that the characteristic frequency at the Hopf bifurcation depends on the capacitance C. We adjust this parameter to obtain the same frequency observed in the experiment. With $C=80$ pF we find good agreement with the experimentally observed frequencies over the full range of time delays, as shown by the dashed line in Fig. 4. The solid line in Figs. 3(a) and 3(b) shows how C limits the bandwidth of the negative resistor. The high frequency roll-off in the reflection coefficient of the model is qualitatively quite similar to the experimental data. The main divergence between the two occurs at frequencies above 100 MHz where the experimental negative resistor acts like a positive resistor with a reflection coefficient near zero whereas the model negative resistor acts like a short circuit with a reflection coefficient of one.

Following the Hopf bifurcation, the new model produces a period-doubling route to chaos. In Fig. 5, we show period 1 [Fig. 5(e)], period 2 [Fig. 5(f)], period 4 [Fig. 5(g)], and chaotic oscillations [Fig. 5(h)]. Thus, the new model reproduces the route to chaos predicted by the model of Eq. (10) and observed experimentally. The full bifurcation sequence occurs over the range of negative resistances from -85 ohms to -75 ohms, somewhat nearer to the observed experimental range (-90 to -80 ohms) than the values of the map model (-120 to -95 ohms). In addition, the new model provides realistic continuous wave forms similar to those observed experimentally. However, there are clearly differences between the simulated and experimental time series. For example, in both the experimental and simulated data, many oscillations include a small amplitude "second bump." These features tend to occur on the leading edge of the oscillation in the experiment while they appear on the trailing edge in the simulation. To more clearly visualize the experimental and simulated attractors we construct a two dimensional delay-embedding space shown in Fig. 7. Despite some difference in appearance between the experimental attractor [Fig. 7(a)] and the simulated attractor [Fig. 7(b)], the two attractors exhibit a common topology, which is even more visible in the return maps, shown in Figs. 7(c) and 7(d). The dynamics on a surface of section through each attractor is approximately describable by a one-dimensional unimodal map, indicating low-dimensional chaos.

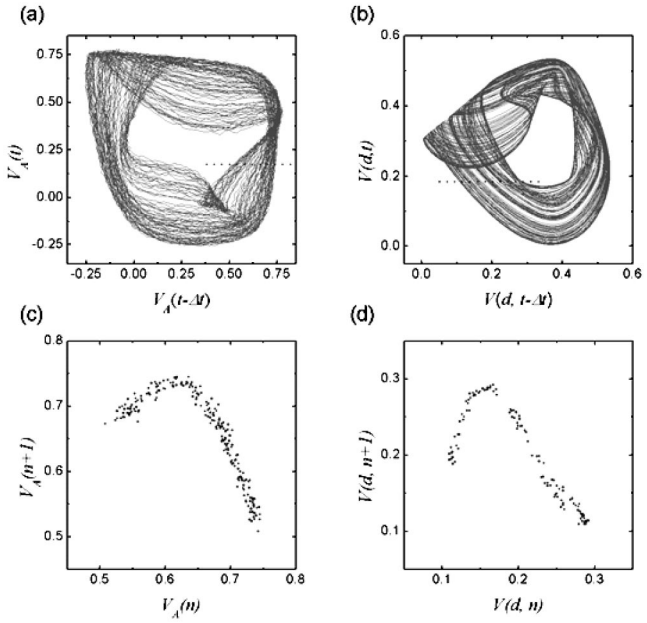

FIG. 7. Phase space reconstructions of the (a) experimental attractor where $R=82.9$ ohms and (b) simulated attractor where $R=75$ ohms. The reconstructed phase space is a time delay embedding with delay $\Delta t=12$ ns. Despite apparent differences between the attractors, their topological similarity is revealed by unimodal return maps extracted from the (c) experimental data and the (d) simulation. The surfaces of section defining the return maps are shown in (a) and (b) as dotted lines.

In choosing a simple model of a negative resistor with finite bandwidth, we have made considerable progress overcoming the limitations of the original map model. However, we recognize that a more detailed model could provide greater insight into the physical mechanisms limiting the response time of the system. For example, the junction capacitance of the diode could be modeled explicitly or a more complicated model of the negative resistor could be introduced. Some positive resistance in series with the current model would give a more realistic high frequency reflection coefficient. These modifications would come at a cost since each additional reactance added to the model raises the order of Eq. (12). Other additions to the model may increase the number of parameters to be measured.

CONCLUSION

We presented the first experimental evidence verifying the predictions of chaotic dynamics in a transmission line terminated with a nonlinear element. We have also introduced an extension of the existing theory that more accurately reproduces the Hopf frequency, bifurcation points, and wave form shapes. The simple architecture of this device and the fact that it naturally incorporates propagation delay (that is inevitable at high speeds) make it well suited for applications of fast chaos. A topic of ongoing investigation is the tailoring of the negative resistor's frequency response in order to obtain chaotic oscillations in a desired frequency band.

ACKNOWLEDGMENTS

This work was performed while J.N.B. held a National Research Council Research Associateship Award at the US Army Research, Development, and Engineering Command. The authors wish to acknowledge fruitful discussions of this work with S. Pethel.

[1] J. N. Blakely, L. Illing, and D. J. Gauthier, IEEE J. Quantum Electron. **40**, 299 (2004).
[2] V. Dronov, M. R. Hendrey, T. M. Antonsen, and E. Ott, Chaos **14**, 30 (2004).
[3] V. S. Udaltsov, L. Larger, J.-P. Goedgebuer, M. W. Lee, E. Genin, and W. T. Rhodes, IEEE Trans. Circuits Syst., I: Fundam. Theory Appl. **49**, 1006 (2002).
[4] J. K. Hale and W. M. Oliva, *Dynamics in Infinite Dimensions* (Springer-Verlag, New York, 2002).
[5] J.-P. Goedgebuer, L. Larger, and H. Porte, Phys. Rev. Lett. **80**, 2249 (1998).
[6] G. D. Van Wiggeren and R. Roy, Phys. Rev. Lett. **81**, 3547 (1998).
[7] I. Fischer, Y. Liu, and P. Davis, Phys. Rev. A **62**, 011801 (2000).
[8] T. Aida and P. Davis, IEEE J. Quantum Electron. **28**, 686 (1992).
[9] B. Mensour and A. Longtin, Phys. Lett. A **205**, 18 (1995).
[10] Z.-R. Zheng, J.-Y. Gao, and P. Dong, IEEE J. Quantum Electron. **36**, 425 (2000).
[11] K. Myneni, T. A. Barr, B. R. Reed, S. D. Pethel, and N. J. Corron, Appl. Phys. Lett. **78**, 1496 (2001).
[12] K. A. Lukin, *The Fourth International Kharkov Symposium on Physics and Engineering of Millimeter and Submillimeter Waves, Kharkov* (IEEE, Piscataway, NJ, 2001), p. 68.
[13] C. P. Silva and A. M. Young, *1998 IEEE International Conference on Electronics, Circuits and Systems, Lisboa, Portugal* (IEEE, Piscataway, NJ, 1998), p. 235.
[14] E. Genin, L. Larger, J.-P. Goedgebuer, M. W. Lee, R. Ferrière, and X. Bavard, IEEE J. Quantum Electron. **40**, 294 (2004).
[15] V. S. Udaltsov, J.-P. Goedgebuer, L. Larger, and W. T. Rhodes, Opt. Commun. **195**, 187 (2001).
[16] J. N. Blakely, L. Illing, and D. J. Gauthier, Phys. Rev. Lett. **92**, 193901 (2004).
[17] A. S. Dmitriev, B. Y. Kyarginsky, A. I. Panas, and S. O. Starkov, Int. J. Bifurcation Chaos Appl. Sci. Eng. **13**, 1495 (2003).
[18] Y. Carmel, W. R. Lou, J. Rodgers, H. Guo, W. W. Destler, V. L. Granatstein, B. Levush, T. Antonsen, Jr., and A. Bromborsky, Phys. Rev. Lett. **69**, 1652 (1992).
[19] R. K. Brayton, Q. Appl. Math. **24**, 289 (1967).
[20] L. Corti, L. DeMenna, and G. Miano, IEEE Trans. Circuits Syst., I: Fundam. Theory Appl. **41**, 730 (1994).
[21] L. Corti, G. Miano, and L. Verolino, Electron. Eng. (Tokyo) **79**, 165 (1996).
[22] G. Miano and A. Malfucci, *Transmission Lines and Lumped Circuits* (Academic, New York, 2001).
[23] A. N. Sharkovsky, IEEE Trans. Circuits Syst., I: Fundam. Theory Appl. **40**, 781 (1993).
[24] J. Kawata, Y. Nishio, and A. Ushida, IEEE Trans. Circuits Syst., I: Fundam. Theory Appl. **44**, 556 (1997).
[25] S. Chowdhury, J. S. Barkatullah, D. Zhou, E. W. Bai, and K. E. Lonngren, IEEE Trans. Circuits Syst., II: Analog Digital Signal Process. **39**, 201 (1992).
[26] J. C. Liao, O. A. Palusinski, and J. L. Prince, *Ninth Annual International Phoenix Conference on Computers and Communications* (IEEE Computer Society, Los Alamitos, CA, 1990), p. 840.
[27] K. Soundararajan and K. Ramakrishna, IEEE Trans. Circuits Syst. **22**, 760 (1975).
[28] A. Namajunas, K. Pyragas, and A. Tamasevicius, Phys. Lett. A **201**, 42 (1995).
[29] G. Mikolaitis, A. Tamasevicius, A. Cenys, S. Bumeliene, A. N. Anagnostopoulos, and N. Kalkan, Chaos, Solitons Fractals **17**, 343 (2003).
[30] K. Ikeda and K. Matsumoto, Physica D **29**, 223 (1987).

[31]D. Farmer, Physica D **4**, 366 (1982).
[32]J. K. Hale, *Theory of Functional Differential Equations*, 1st ed. (Springer-Verlag, New York, 1977).
[33]A. G. Balanov, N. B. Janson, P. V. E. McClintock, R. W. Tucker, and C. H. T. Wang, Chaos, Solitons Fractals **15**, 381 (2003).
[34]W. H. Press, B. P. Flannery, S. A. Teukolsky, and W. T. Vetterling, *Numerical Recipes in C: The Art of Scientific Computing* (Cambridge University Press, Cambridge, 1988), Chap. 16, p. 747.